Contributions of Janbu and Lade as applied to Reinforced Soil

Peter Hoffman
Reinforced Soil Research Center, Department of Civil Engineering
University of Colorado Denver, USA, peter.hoffman@ucdenver.edu

ABSTRACT
The expression for Young's Modulus of soil was developed by Janbu [1963] and refined by Lade [1987]. Analogous to reinforced concrete, reinforced soil behavior is characterized by a modular ratio, that is, by the modulus of soil relative to the modulus of reinforcement. With reliance upon these contributions of Janbu and Lade, the capacity and deformation of reinforced soil structures are calculated. These calculations are validated with test data from the U.S. Federal Highway Administration.

Keywords: reinforced soil, elastic, plastic, steel, geosynthetic

1 INTRODUCTION

Without an equation due to Janbu and Lade, deformation of reinforced soil cannot be calculated. This equation is also used in the capacity calculation of steel reinforced soil.

Hooke's law, in Section 2, is fundamental to elastic and plastic calculations. Section 3 explains shear lag in construction materials. Section 4 elaborates on the equations of Janbu and Lade for Young's modulus in soil.

Section 5 shows that geosynthetic reinforced soil exhibits plastic behavior while steel reinforced soil remains elastic. Details of the calculation are relegated to the Appendix, but the "quad chart" is introduced to characterize behavior.

Section 6 validates the calculations and the quad chart.

2 MECHANICS OF REINFORCED SOIL

Poisson's ratio plays a primary role in reinforced soil: vertical compression causes horizontal extension, which mobilizes the reinforcement and increases confining pressure. Elasticity, which always prevails at small loads, determines whether plasticity occurs at large loads in a reinforced soil composite. The compacted engineered fill of a structure is homogeneous, isotropic, and elastic, and it follows from Hooke's law

$$\varepsilon_x = \frac{1}{E}\left[\sigma_x - \nu\left(\sigma_y + \sigma_z\right)\right] \qquad (1)$$

that, for a square or round pier,

$$\frac{K}{K_A} = \frac{K_P}{2 + 2.25W\dfrac{E_S}{E_R}} \qquad (2)$$

where K/K_A is a parameter used by the American Association of State Highway and Transportation Officials (AASHTO); otherwise, K_A and K_P would be eliminated.

Equation (2) assumes an aggregate that drains well, has negligible cohesion, and has a Poisson's ratio of approximately $\nu = 1/3$. $K = \sigma_H/\sigma_V$ during elastic deformation while $K_A = \sigma_3/\sigma_1$ is the ratio of principal stresses at plastic yield. K_A is the coefficient of active lateral earth pressure, and K/K_A measures the mobilization *(M)* of confining pressure. Elasticity is associated with $K/K_A > 1$, and plasticity with $K/K_A < 1$. $1/K_A = K_P = \tan^2 \alpha_f$, where $\alpha_f = 45° + \phi/2$ is the failure angle and $\phi = \phi'$ is the effective stress friction angle. Analogous to reinforced concrete, the modular ratio E_S/E_R compares soil stiffness and reinforcement stiffness within the

reinforced layer. Shear lag is associated with *W*. Equation (2) also applies to piers when '2.25' is increased to '3', which reduces stiffness.

The parameters *W* and E_S are examined in the next sections.

3 SHEAR LAG AND *W*

Shear lag in reinforced soil is measured by *W*. Shear lag limits the effectiveness of beams with wide flanges. Steel and concrete beams carry less stress at the flange tip than at the web. Similarly, soil contributes less confining pressure at the middle of a soil layer than at the reinforcement.

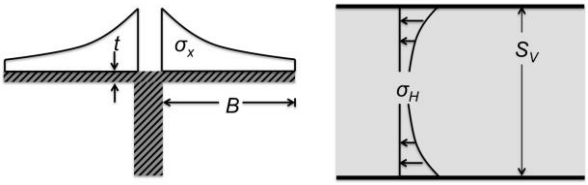

(a) (b)

Figure 1 Shear lag in (a) beams is analogous to shear lag in (b) reinforced soil.

In a beam, shear lag is determined by the ratio *B*/*t* of flange width and thickness. In sheet reinforced soil, shear lag is determined by the ratio S_V/D_{max} of reinforcement spacing and soil particle diameter (Pham 2009, Adams et al. 2011, Wu and Pham 2013).

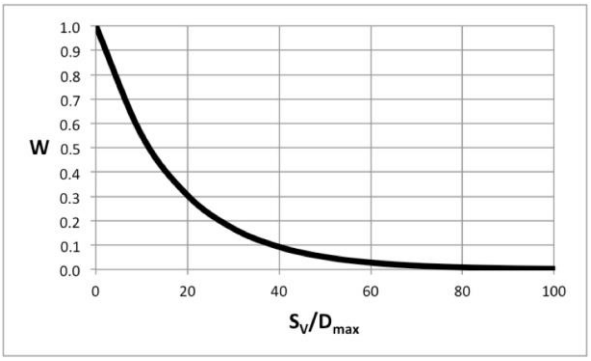

Figure 2 Shear lag is measured by W, a function of sheet spacing and soil particle size.

With strip reinforcement rather than sheets, *W* would be much smaller. The US Federal Highway Administration (FHWA) validated the phenomenon of shear lag in geosynthetic reinforced soil. In a series of tests, FHWA loaded faced and unfaced piers to ultimate capacity (Nicks et al. 2013).

(a) (b)

Figure 3 FHWA tested both (a) faced piers and (b) unfaced piers to ultimate capacity.

Using *W*, capacity is calculated with the Lower Bound Theorem of plasticity theory. Validating *W*, FHWA data show that measured capacities agree with calculated capacities, $Q_{ult} = K_P T_f / S_V$ for faced piers and $q_{ult} = WQ_{ult}$ for unfaced piers. T_f is tensile strength of sheet reinforcement, and S_V is its vertical spacing. Facings withstand lateral pressure of $K_A Q_{ult}$ (Wu and Payeur 2014).

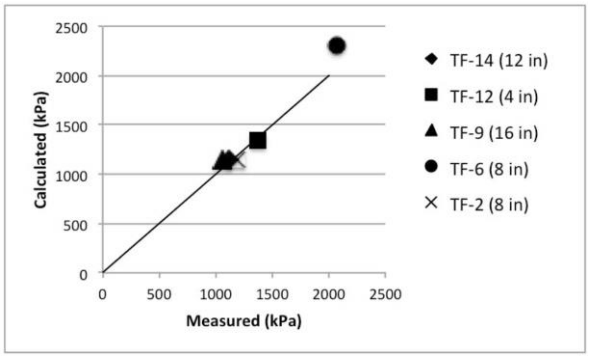

(a)

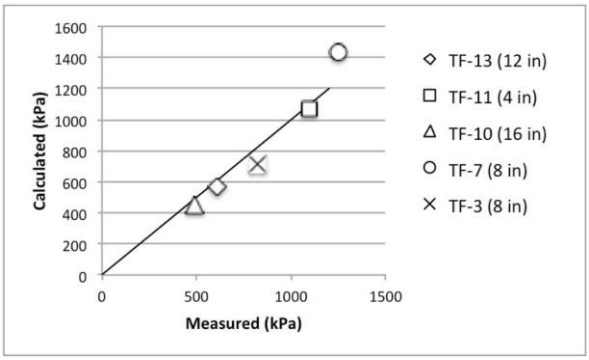

(b)

Figure 4 Validating W, measurements agree with calculated capacities (a) Q_{ult} for faced piers and (b) $q_{ult} = WQ_{ult}$ for unfaced piers.

4 JANBU, LADE, AND E_S

E_S, the Young's modulus of soil, is required by Equation (2) for calculation of K/K_A. More precisely, E_S is required in order to determine

- capacity of soil reinforced with steel
- deformation of soil reinforced with either steel or geosynthetics

Showing experimental insight, Janbu (1963) provided the well-known expression

$$E_S = Kp_a\left(\frac{\sigma}{p_a}\right)^n \qquad (3)$$

where σ is lateral confining pressure and p_a is atmospheric pressure. Parameters K and n are specific to a soil.

Figures 5 and 6 show Janbu's plots, slightly adapted. Figure 5 shows that $K \approx 500$ for aggregates. Figure 6 indicates that $n = 0$ for solid rock, $n = 1$ for wet clay, and n ≈ 0.5 for aggregates.

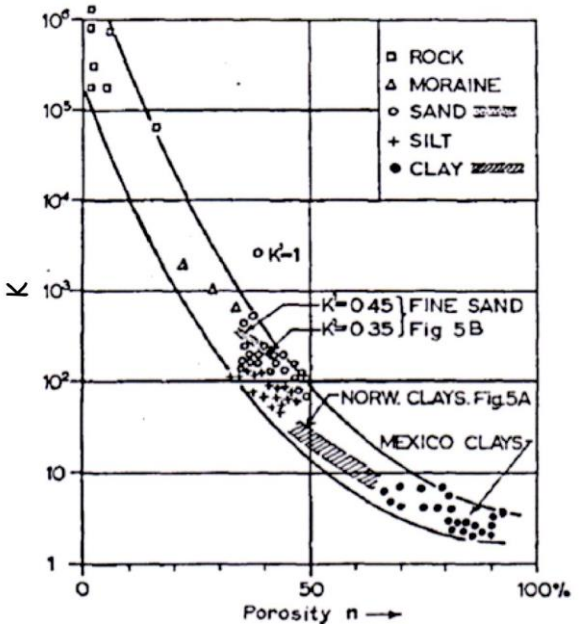

Figure 5 Janbu's data show that K ≈ 500 for aggregates.

Equation (3) poses difficulties. Strain energy is not conserved around load paths that are closed loops involving shear as well as confining pressure.

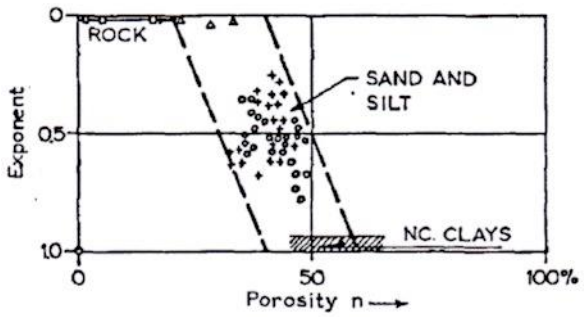

Figure 6 Janbu's data show that n ≈ 0.5 for aggregates.

With analytical elegance, Lade (1987) incorporated shear into the equation

$$E_S = Kp_a\left(\frac{\sqrt{p^2 + rq^2}}{p_a}\right)^n \qquad (4)$$

through the tensor invariants, $p = I_1/3$ for the hydrostatic pressure and $q = \sqrt{J_2}$ and for the deviatoric stress. Then, r is a function of Poisson's ratio only.

While Janbu's approach was entirely experimental, Lade's was totally analytical, using advanced calculus and assuming only the definition of strain energy.

Amazingly, the elastic constant K can be determined from the plastic constant K_P because the elastic zone touches the plastic yield surface in stress space. This enables K to be written as a function of K_P. Observe that $2p = (K_P + 1)\ \sigma_3$ and $2q = (K_P - 1)\ \sigma_3$ in two dimensions. Duncan et alia (1978) published data for 30 aggregates, which are compiled from several laboratories. The best fit is $K = 100\ K_P$, which is consistent with Janbu's $K \approx 500$ for aggregates in Figure 7.

Janbu's data also show that $n \approx 0.5$ for aggregates. This fact is easily shown mathematically for small strains. Because E is presumably a smooth function of strain ε when there is no plasticity (no clay), its Taylor expansion is $E = a_o + a\varepsilon = a\sigma/E$ when cohesion is zero. So, E is proportional to $\sigma^{1/2}$.

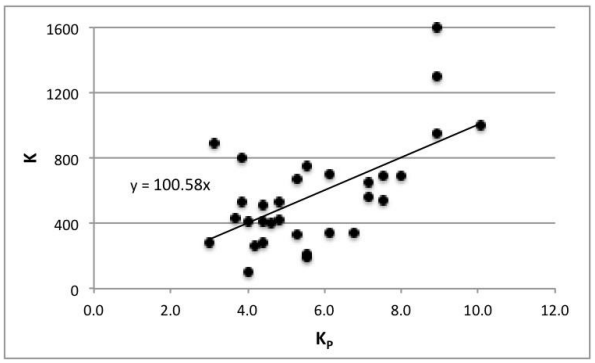

Figure 7 The data show that $K \approx 100\ K_P$ for aggregates.

In summary,

$$E_S = 100 K_P p_a \left(\frac{\sigma_3}{p_a} \right)^{0.5} \qquad (5)$$

is used with Equation (2) and with $\sigma_3 = \sigma_H$ in order to calculate the mobilization $M = K/K_A$.

5 APPLICATION

Consider a square reinforced soil pier with

- 70 kN/m = T_f (sheet tensile strength of reinforcement)
- 0.2 m = S_V (vertical spacing of reinforcement)
- 45° = ϕ (friction angle of soil)
- 0.013 m = D_{max} (diameter of large soil particles)
- 10% & 0.25% = ε_R (extensibility for geosynthetic and steel, respectively)

Extensibility is strain in the reinforcement as T_f is reached. The Appendix provides the detailed calculation. As shown in Figure 8, steel and geosynthetics give reinforced soils that behave quite differently. With ε_R = 3%, fiberglass lies between them and is being installed for reinforced soil foundations beneath commuter rail tracks in the US.

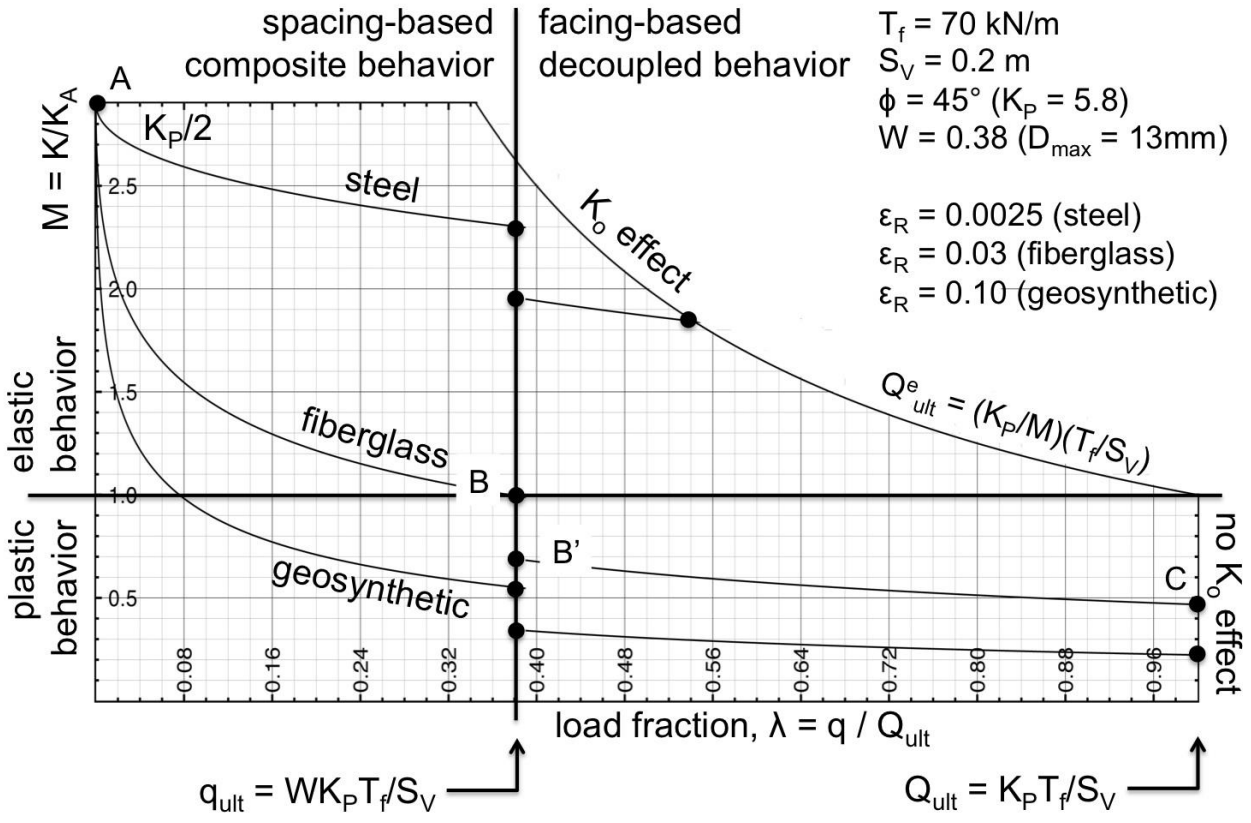

Figure 8 Due to extensibility, geosynthetic reinforced soil behaves quite differently from steel reinforced soil. Between steel and geosynthetic, fiberglass behaves nicely. Lines M =1 and λ = W divide the chart into four quadrants, each with unique attributes. The maximum value is $M = K_P/2$.

At ultimate capacity, both elastic and plastic deformation are present in the geosynthetic reinforced soil. Elastic strain is calculated from E_S. Plastic strain is calculated from the mobilization, $M = K/K_A$, by Figure 9.

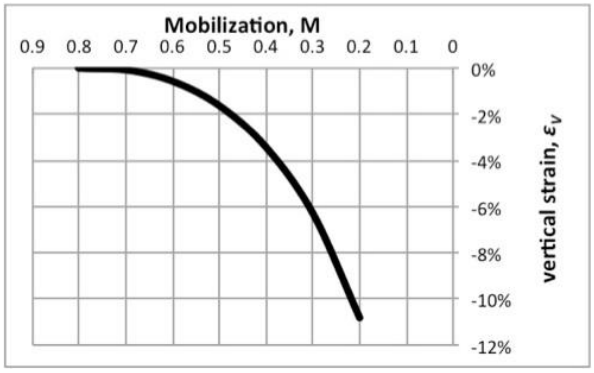

Figure 9 Mobilization, $M = K/K_A$ determines vertical strain due to plasticity.

Figure 9 is derived on the premise that plastic slip accommodates the shortage of mobilized elastic strength when $K < K_A$ (Hoffman and Wu 2015). The derivation uses plasticity theory in the tradition of Prandtl and Sokolovskii before non-associated plastic potentials. The yield surface is drawn in stress space, and in the derivation, the plastic potential is the yield surface drawn in Euclidean space. Stress space distorts geometry, and yield surfaces appear too wide and too strong. For example, lines with slope $\sqrt{K_A}$ or $\sqrt{K_P}$ in Euclidean space have slope K_A or K_P in stress space.

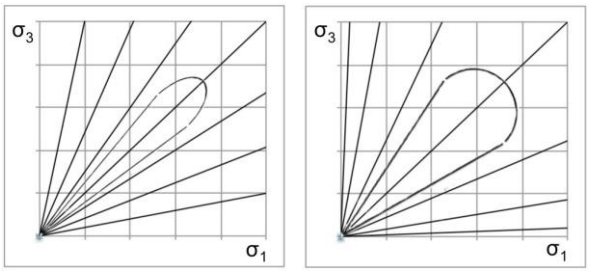

(a) (b)

Figure 10 Compared to (a) Euclidean space, (b) stress space σ_1-σ_3 distorts geometry.

6 VALIDATION

The four quadrants of Figure 8 exhibit individual behaviors. When $K/K_A < 1$, the structure exhibits plastic deformation because soil stiffness exceeds reinforcement stiffness in the sense of Equation 2. When the spacing-based capacity is exceeded, transition occurs as the core of the soil layer decouples from the reinforcement and presses against the facing; therefore, bulging and creep appear.

composite elastic 2	1 decoupled elastic
composite plastic 3	4 decoupled plastic

Figure 11 Attributes of the four quadrants

Examples are now provided for each of the four quadrants.

6.1 First Quadrant

With its curved boundary, the first quadrant appears strange. For steel reinforced soil, capacity involves division by M where $M > 1$, and the curve results from that division.

Poorly-behaved steel reinforced soil lies in the first quadrant. For validation, consider the SS3 steel strip wall constructed at Vicksburg in the USA (Allen et al. 2001). As indicated in Figure 12, failure of SS3 coincides with the quadrant's calculated boundary.

Prior to failure, "significant bulging" was reported for SS3.

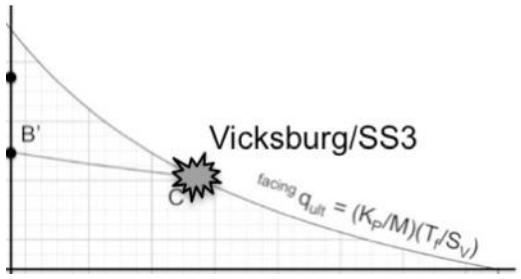

Figure 12 Failure of SS3 lies on the quadrant's calculated boundary. "Significant bulging" preceded failure.

6.2 Second Quadrant

Well-behaved steel reinforced soil structures lie in the second quadrant. As Figure 13 illustrates, their K/K_A curves rise steeply. Consider the welded wire fabric wall, WW1, constructed on I-90 at Rainier Avenue in

Seattle (Bathurst et al. 2009). Figure 13 compares calculations, measurements, and the design curve of the AASHTO Simplified Method (Anderson et al. 2012, Bathurst et al. 2009). The bends in the curves reflect transition between the first and second quadrants.

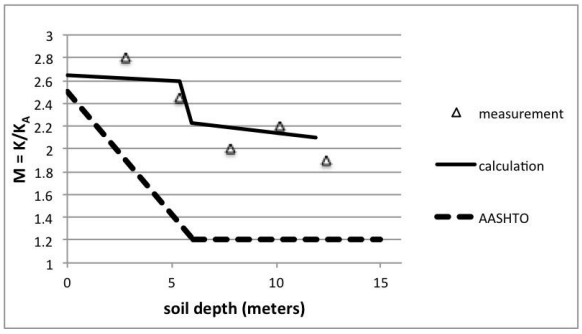

Figure 13 Measurements, calculations, and AASHTO's Simplified Method are compared for welded wire fabric wall WW1.

6.3 Third Quadrant

Well-behaved geosynthetic reinforced soil structures lie in the third quadrant. Consider four early pier tests by Defiance County, Ohio (USA) and FHWA (Adams et al. 2011). Values of K/K_A are calculated, converted to deformations, and compared with test data in Figure 14.

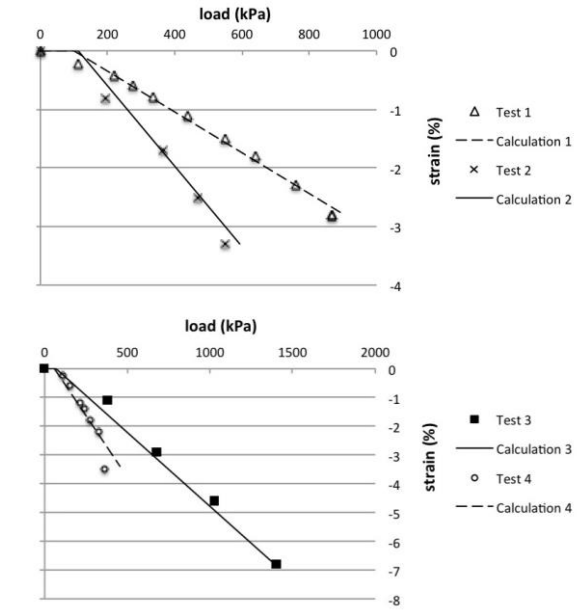

Figure 14 Calculations and measurements for four early pier tests, where load ≤ q_{ult} = WQ

In Figure 14, the final test data point departs from the line in each case. This reflects the onset of transition between the third and fourth quadrants. Increased facing pressure is also associated with transition.

Since 2011, FHWA has upgraded to measure ultimate capacities at very large strains. In Figure 15, transition at $q_{ult} = WQ_{ult}$ (near 500 kPa) is validated by FHWA Tests TF-9 and TF-10 (Nicks et al. 2013). These are faced and unfaced tests with 0.4 m (16 inch) spacing. Large strains are unacceptable in construction, but they reveal behavior and validate the quad chart for reinforced soil.

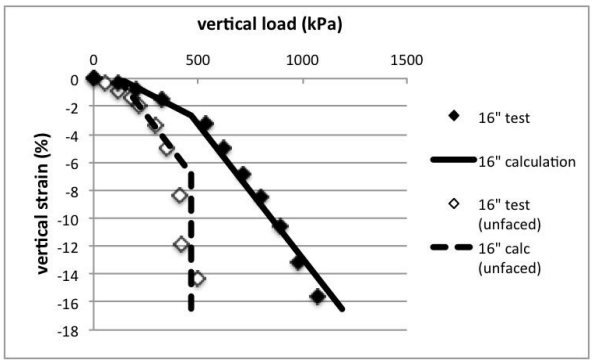

Figure 15 Transition at $q_{ult} = WQ_{ult}$ (near 500 kPa) is validated for faced/unfaced pair of piers.

6.4 Fourth Quadrant

Creep occurs in this quadrant:

- CDOT/aggregate - one of several creep tests conducted by CU Denver and the Colorado DOT (Ketchart and Wu 1996)
- I-90 temp/Seattle - GW16 existed for one year during construction (Allen and Bathurst 2003)
- Japan/GW35 - test wall built by the Public Works Research Institute (Bathurst et al, 2008)
- Yeager Airport - disaster in March 2015 destroyed a 50-home community in West Virginia (Lostumbo 2010). This soil structure predates the publication of shear lag research for reinforced soil.

Figure 16 displays the four creep cases in quad chart format.

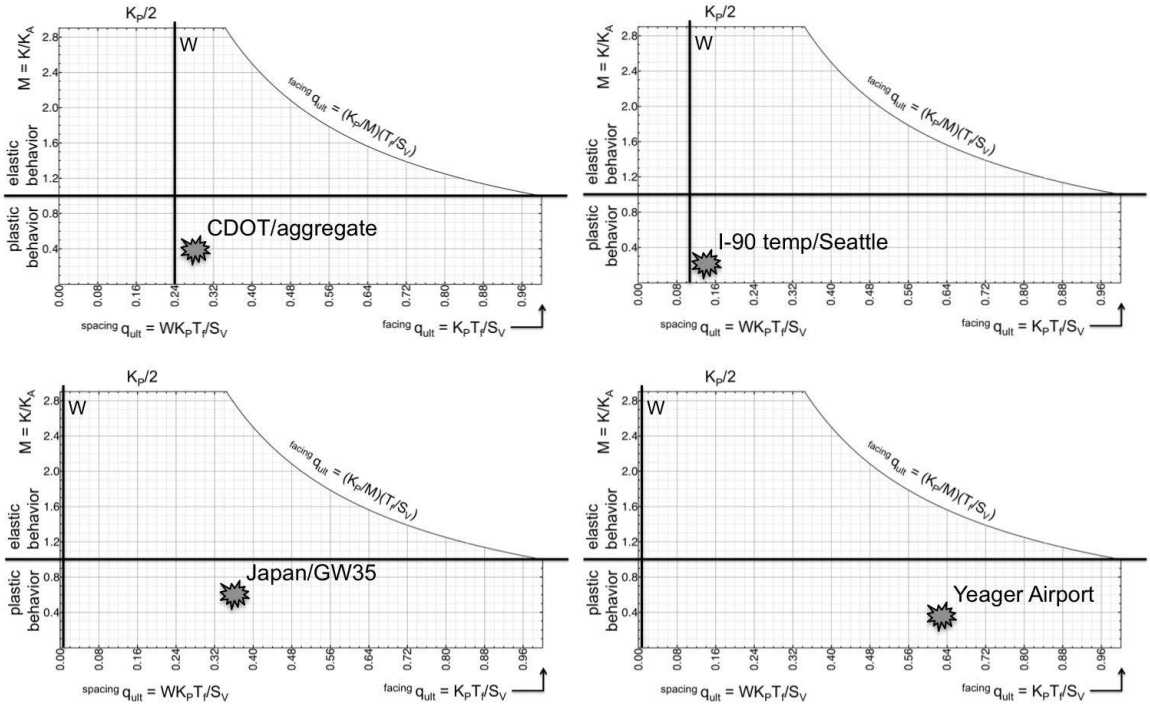

Figure 16 Known cases of creep are right of the transition or W-line.

7 CONCLUSIONS

Increasingly, reinforced soil lurks as a threat within the infrastructure. Collapse of the 75 meter geogrid structure at Yeager Airport (USA) destroyed a 50-home community in 2015. Failures of many small structures are incorrectly attributed to water, which is a secondary cause or accelerant. Bulging and serviceability problems are abundant.

Critical issues are characterized by the quad chart introduced in Section 5. Behavior is determined by shear lag and by the modular ratio between soil stiffness and reinforcement stiffness. Without Janbu and Lade, we would not understand this modular ratio. Their contributions are essential to the quad chart. Their equations reveal that behavior of steel reinforced soil is elastic while behavior with geosynthetics is plastic and quite different.

Safety demands maturity for reinforced soil. Maturity of the industry can be and should be raised toward the level of maturity achieved for reinforced concrete.

8 APPENDIX

The calculation of $M = K/K_A$ uses the method of Hoffman and Wu (2015). Although values can be calculated for any load, they are calculated here for ultimate capacity q_{ult} at its Point B, immediately left of the transition or *W*-line. The calculation is performed here for a geosynthetic wall or abutment.

As in reinforced concrete, Equation 2 reveals the importance of the modular ratio, E_S/E_R. For reinforcement, E_R involves the extensibility ε_R, which is perhaps the most critical parameter in reinforced soil design. For soil, E_S is determined by Equation 5, but confining pressure σ_H must first be estimated.

$$\begin{aligned} \sigma_H^{\max} &= MK_A q_{ult} \\ &= MK_A K_P W T_f / S_V \\ &= MWT_f / S_V \end{aligned} \qquad (6)$$

The average is obtained by evaluating E_S at 0.44 $\sigma_H^{\max}$, not 0.50 $\sigma_H^{\max}$, because of the square root in Equation 5. Thus,

$$\sigma_H = 0.44 M W T_f / S_V \quad (7)$$

$M = K/K_A$ is found by simultaneous solution of Equations 2, 5, and 7.

Parameters for the geosynthetic are T_f = 70 kN/m, S_V = 0.2 m, ϕ = 45°, D_{max} = 13 mm, and ε_R = 10%. At best, they are accurate to two decimal places, and the calculations of this appendix keep two digits of accuracy.

First, the intermediate parameters are

$$K_P = \tan^2\left(45° + \phi/2\right) = 5.8 \quad (8)$$

$$W = 0.7^{S_V / 6D_{\max}} = 0.39 \quad (9)$$

$$E_R = \frac{T_f}{\varepsilon_R S_V} = 3500 \text{ kPa} = 3.5 \text{ MPa} \quad (10)$$

Then, the three equations for $M = K/K_A$ at Point B are

$$\sigma_H = 0.44 M W T_f / S_V = 60M \text{ kPa} \quad (11)$$

$$E_S = 100 K_P \sqrt{p_a}\sqrt{\sigma_H} \text{ kPa} = K_P \sqrt{\sigma_H} \text{ MPa} = 5.8\sqrt{\sigma_H} \text{ MPa} \quad (12)$$

$$M = K_P / \left(2 + 2.25 W \frac{E_S}{E_R}\right) = 5.8/\left(2 + 0.25 E_S\right) \quad (13)$$

The system is solved by iteration in Table 1.

Table 1 Iteration for Point B of geosynthetic

Equation	iter 1	iter 2	iter 3	iter 4
$\sigma_H = 60M$ kPa	60	43	37	34
$E_S = 5.8\sqrt{\sigma_H}$ MPa	45	38	35	**34**
$M = 5.8/\left(2 + 0.25E_S\right)$	.44	.50	.54	.55
(M_{init} = 1.0) $M_{average}$:	.72	.61	.57	**.56**

Two successive values of M are averaged in order to stabilize the iteration. $M = K/K_A$ = 0.56 is plotted in Figure 8.

E_S = 34 MPa is highlighted in Table 1 as it can be used to calculate elastic deformation. With extensibility ε_R = 0.25%, steel gives $M = K/K_A$ = 2.3 at Point B. At 3%, fiberglass is well-behaved with $M = K/K_A$ = 1.0.

9 REFERENCES

Adams, M.T., Nicks, J., Stabile, T., Wu, J.T.H., Schlatter, W. and Hartmann, J. (2011). Geosynthetic Reinforced Soil Integrated Bridge System – Interim Implementation Guide. Report No. FHWA-HRT-11-026, Federal Highway Administration, Washington, DC.

Allen, T.M, Christopher, B., Elias, V., and DiMaggio, J. (2001) Development of the Simplified Method for Internal Stability of Mechanically Stabilized Earth Walls. Report WA-RD 513.1, Washington State Department of Transportation, Olympia.

Allen, T.M., and Bathurst, R.J. (2003). Prediction of Reinforcement Loads in Reinforced Soil Walls. Report WA-522.2, Washington State Department of Transportation, Olympia, WA.

Anderson, P.L., Gladstone, R.A., and Sankey, J.E. (2012). State of the Practice of MSE Wall Design for Highway Structures, Geotechnical Engineering State of the Art and Practice: Keynote Lectures for GeoCongress 2012, Oakland, CA.

Bathurst, R.J., Miyata, Y., Nernheim, A., and Allen, A.M. (2008), Refinement of K-stiffness Method for Geosythetic-reinforced Soil Walls, Report HIIFP-095j , Highway Infrastructure Innovation Funding Program, Ontario Ministry of Transportation.

Bathurst, R.J., Nernheim, A., and Allen, T.M. (2009). Predicted Loads in Steel Reinforced Soil Walls Using the AASHTO Simplified Method, J. Geotech. Geoenviron. Eng. ASCE 135, 177-184.

Duncan, J.M., Byrne, P., Wong, K.S., and Mabry, P. (1978). Strength, Stress-Strain and Bulk Modulus Parameters for Finite Element Analysis of Stresses and Movements in Soil Masses. Report No. UCB/GT/78-02, University of California, Berkeley.

Hoffman, P.F., and Wu, J.T.H. (2015). An Analytical Model for Predicting Load-Deformation Behavior of the FHWA GRS-IBS Performance Test, International Journal of Geotechnical Engineering, Vol 9, Issue 2: 150-162.

Janbu, N. (1963). Soil Compressibility as Determined by Oedometer and Triaxial Tests, European Conference on Soil Mechanics and Foundation Engineering, Wiesbaden, Germany, Vol. 1, pp. 19-25.

Ketchart, K., and Wu, J.T.H. (1996). Long-Term Performance Tests of Soil-Geosynthetic Composites Report No. CDOT-CTI-96-1, Colorado Department of Transportation, Denver.

Lade, P.V., and Nelson, R.B. (1987). Modelling the Elastic Behavior of Granular Materials, International Journal for Numerical and Analytical Methods in Geomechanics, 11, 521-542.

Lostumbo, J.M. (2010). Yeager Airport Runway Extension, Presented at the 2010 Southeastern Transportation Geotechnical Engineering Conference (STGEC), Charleston, WV.

Nicks, J.E., Adams, M.T., and Ooi, P.S.K. (2013). Geosynthetic Reinforced Soil Performance Testing: Axial Load Deformation Relationships, Report No. FHWA-HRT-13-066, Federal Highway Administration, McLean, VA.

Pham, T. Q. (2009). Investigating Composite Behavior of Geosynthetic-Reinforced Soil (GRS) Mass. Ph.D. Dissertation, University of Colorado Denver.

Wu, J.T.H., and Payeur, J-B. (2014). "Connection Stability Analysis of Segmental Geosynthetic Reinforced Soil (GRS) Walls." *Transportation Infrastructure Geotechnology*, 2(1). DOI 10.1007/s40515-014-0013-4.

Wu, J.T.H. and Pham, T.Q (2013). Load Carrying Capacity and Required Reinforcement Strength of Closely Spaced Soil-Geosynthetic Composites, J. Geotech. Geoenviron. Eng. ASCE 139(9), 1468–1476.